F. Edemetti, et al., Optimization of the First Wall cooling system for the DEMO WCLL blanket, Fusion Engineering and Design, 2020, https://doi.org/10.1016/j.fusengdes.2020.111903

Optimization of the First Wall cooling system for the DEMO WCLL blanket

Francesco Edemetti [a*], Pietro Micheli [a], Alessandro Del Nevo [b], Gianfranco Caruso [a]

[a] *Department of Astronautical, Electrical and Energy Engineering, Sapienza University of Rome, Roma, Italy*
[b] *ENEA FSN-ING-PAN, ENEA CR Brasimone, Camugnano, Italy*

The Water-Cooled Lithium-Lead (WCLL) Breeding Blanket (BB) is a key component in charge of ensuring Tritium production, shield the Vacuum Vessel and remove the heat generated by plasma thermal radiation and nuclear reactions. It relies on PbLi eutectic alloy adopted as breeder and neutron multiplier and refrigerate by subcooled pressurized water. The last function is fulfilled by two independent cooling systems: First Wall (FW) that faces the plasma heat flux and the Breeding Zone (BZ) that removes the deposited power of neutron and photon interaction.

Several layouts of WCLL BB system have been investigated in the last years to identify a configuration that guarantees Eurofer temperature below the limit (550°C) and good thermal-hydraulic performances.

This research activity focuses on the FW cooling system based on the WCLL BB 2018 design of DEMO 2017 baseline, investigating the cooling performances in order to optimize the FW design, reducing the amount of water that affects the Tritium Breeding Ratio (TBR) and improves the efficiency of the Primary Heat Transfer System (PHTS), verifying the reliability to deliver coolant at adequate design temperature (328°C) to the PHTS. Different solutions have been considered and analyzed focusing on three specific positions along the poloidal direction: the equatorial cells in the Central Outboard Segment (COB) and Inboard Segment (IB), where there is the maximum deposited power and low Heat Flux (HF), and the apical cell of the IB, impacted by the highest HF but with low deposited power. For each FW design, several thermal-hydraulic steady-state analyses have been performed, as well as sensitivity analyses to evaluate the response of the systems under different cooling configuration, changing the position and the number of channels. Furthermore, a transient analysis reproducing the Dwell-Pulse phase of the DEMO fusion reactor with the optimized configuration of the Outboard FW layout has been performed to study the behavior of the FW cooling system subjected to the pulsed operation.

The research activity aims at laying the basis for the finalization of the WCLL BB design, pointing out relevant thermal-hydraulic aspects. The analyses have been carried out using a CFD approach, thus a 3D finite volume model of each configuration has been developed, adopting the commercial ANSYS CFX code. The goal of the study is to compare the different FW cooling system layouts, identifying and discussing advantages and key issues from the thermal-hydraulic point of view. The results show that the coolant system of FW can safely remove the high plasma HF and nuclear heat deposition with a reduction of water channels, delivering coolant to the FW PHTS heat exchanger at the design temperature.

Keywords: WCLL, CFD, FW System, Breeding Blanket, Blanket Engineering.

1. Introduction

The Water-Cooled Lithium Lead (WCLL) Breeding Blanket (BB) is a candidate breeding blanket for DEMO fusion power plant [1]. It must ensure an adequate neutron shielding, tritium breeding self-sufficiency, and energy extraction for electricity production. Lithium Lead (PbLi) is adopted as breeder, neutron multiplier and tritium carrier, Eurofer as structural material, and pressurized water at typical Pressurized Water Reactor (PWR) conditions (15.5 MPa) as First Wall (FW) and Breeding Zone (BZ) coolant. The WCLL BB is designed according to the Single Module Segment (SMS) approach, based on DEMO 2017 baseline, subdivided into 16 sectors, each of them covering a toroidal angular extent of 22.5°. Each of these sectors is composed of three Outboard segments (OB) and two Inboard segments (IB) [2]. To guarantee adequate mechanical properties, the Eurofer must be cooled at a temperature lower than 550°C during the normal operation [3][4].

The thermal-hydraulic studies have the responsibility to evaluate and to provide an adequate temperature distribution of the BB verifying the maximum temperature of Eurofer structures, to investigate PbLi heat transfer coefficient in the BZ and to predict the thermal performances of BZ and FW coolant systems. The analyses are focused on the WCLL FW cooling system, regarding the IB and OB. A detailed three-dimensional model of the FW is developed, analyzing three different FW cooling system placed in different positions: Central Outboard Segment (COB) equatorial cell, IB equatorial cell, and IB apical cell. In particular, the first and the second locations have the highest volumetric power deposition and lowest Heat Flux (HF) on the plasma-facing surface whereas, conversely, the third one is characterized by the highest HF and lowest volumetric deposited power.

The main objective of this study is to optimize the channels layout of different FW systems by reducing the number of channels and, indeed, the amount of water in the first centimeters of the elementary cells, that affects in a negative way

author's email: francesco.edemetti@uniroma1.it

the Tritium Breeding Ratio (TBR), because of neutrons thermalization and consequent reduced interaction with the breeder, but ensuring adequate refrigeration of the Eurofer structures. Moreover, the analysis is aiming to increase water performance in order to obtain adequate thermodynamic conditions for the PHTS heat exchanger.

Moreover, a transient analysis is performed on a simplified COB equatorial elementary FW system cooled by two water channels in counter current flow, due to the periodicity of the FW, to simulate the Dwell-Pulse phase of DEMO, aimed at analyzing the capability of the system to provides adequate cooling during this operation phase.

2. DEMO WCLL BB 2018

Starting from the main outcomes obtained from WCLL 2018 design and analyses [5][6][7], a different optimized design has been developed in 2019.

The WCLL BB 2018 consists of the FW, an external box of Eurofer water-cooled by counter current square channels with a Tungsten layer that faces the plasma, and the BZ, an internal box filled with liquid PbLi alloy. The PbLi flows through channels defined by structural stiffeners and cooled by Double Wall Tubes (DWTs). The BZ is reinforced by stiffening plates to safely withstand the thermo-mechanical loads postulated in normal, off-normal and accidental conditions. The stiffening approach constrains the breeder flow in a radial-poloidal-radial path: it enters from the bottom part through holes and exits from the top part of the cell. In Fig. 1 the isometric view of the IB and COB equatorial elementary cell are shown.

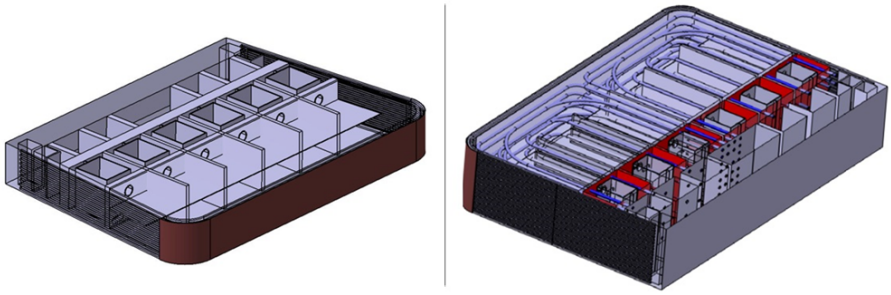

Fig. 1: WCLL BB concept: isometric views of IB (left) and COB (right) elementary cell

Regarding the FW system, it is composed by a U-shaped structure 25 mm thick, bent in the radial direction, while the plasma-facing surface is coated by a 2 mm Tungsten armor. The water flows in counter–current inside 7x7 mm channels. The FW system has the following tasks: to deliver coolant to the PHTS at the design temperature (i.e. 328°C at 15.5 MPa), to remove the volumetric deposited power into the system, not exceeding the Eurofer temperature limit of 550°C, and also to remove the surface heat load related to the plasma operation that directly impacts the Tungsten armor. In Fig. 2, a sketch of the FW cooling system is shown.

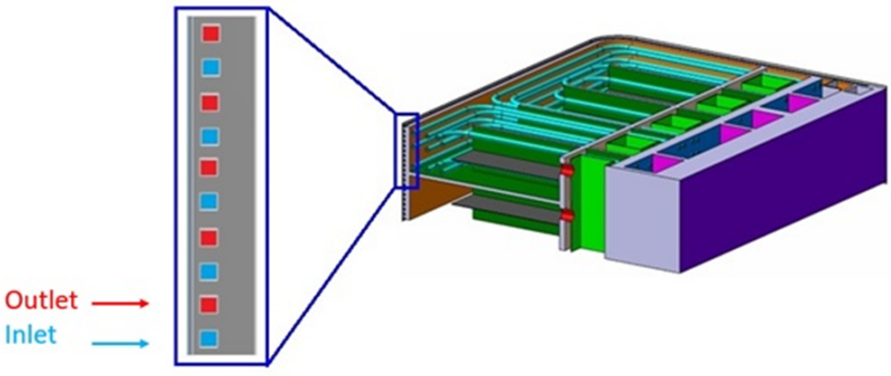

Fig. 2: WCLL FW system counter current flow path

Since the analysis aims to investigate different part of the WCLL BB FW system in different positions along the poloidal direction, each model has different geometric dimensions and is subjected to different heat loads.

2.1. FW COB equatorial models

The COB equatorial blanket has a toroidal length of 1500 mm and radial dimension of 1000 mm. In the present analysis, the poloidal dimension of the model is clipped to a height of 135 mm, which is representative of a single BZ elementary cell. Moreover, the model radial dimension is reduced to 567 mm, thus neglecting the FW section covering the manifold and back supporting structure, where heat loads are foreseen to be negligible.

Three models with different channels layout are evaluated for steady-state analyses, varying the number of the channels and their pitch. The first numerical model is based on the reference layout of the FW system, with 10 square channels arranged along the poloidal direction and a uniform pitch of 6.5 mm [5][6]. The second and third configurations foresee 6 and 4 channels, with a constant pitch of 15.5 mm and 26.75 mm respectively. In Fig. 3 the three different configurations of the COB equatorial cell are reported.

Regarding the transient analysis, a simplified configuration of the 4 channels layout has been adopted. The geometry has been reduced to two water channels, due to the periodicity of the system, to optimize the computational cost of the analysis.

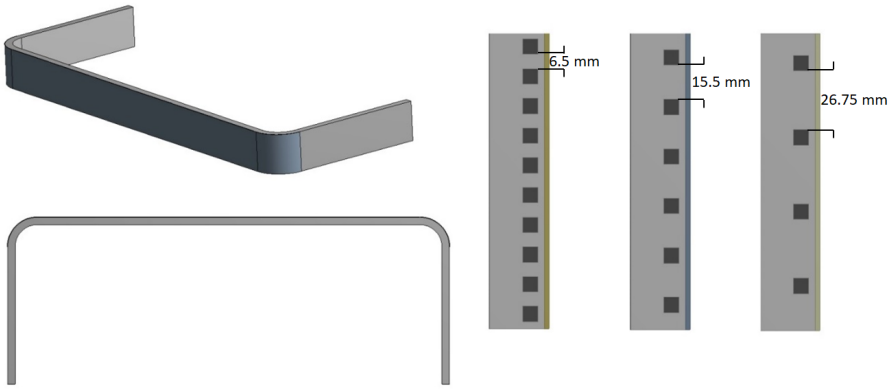

Fig. 3: WCLL FW system COB equatorial model with different number of channels

2.2. FW IB equatorial models

The IB equatorial system has smaller dimensions than COB, having a toroidal width of 1127 mm and a radial dimension length of 800 mm. As for the COB system, the model is realized to account for a single BZ elementary cell and, therefore, it is limited to a 364 mm radial length and 135 mm of total height. Conversely to the COB, the elbows are curved inwards with an angle slightly larger than 90°, reaching 95°.

In this case, only two alternatives configurations are investigated. The first one is the reference layout with 10 water channels, whereas the second features 4 water channels only. Both solutions have the water channels equally distributed along the poloidal height with a 6.5 mm and 26.75 mm pitch, respectively. In Fig. 4, the model geometry and the two channels layout are shown.

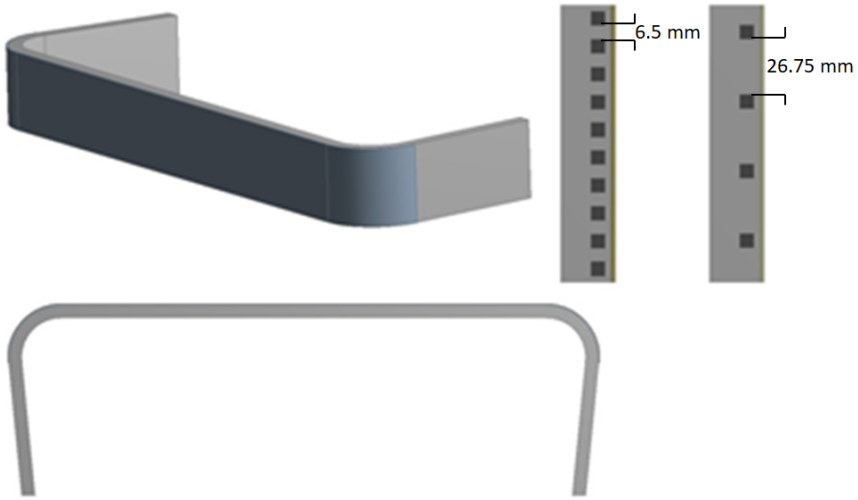

Fig. 4: WCLL FW system IB equatorial model with different number of channels

2.3. FW IB apical models

The IB apical system has a more complex geometry, since it does not follow a toroidally rectilinear course, but rather slightly twists along the toroidal path of the FW. Even the radial side walls are asymmetric, with different curvature radius in the poloidal and toroidal directions. The poloidal height is also not regular, as it differs slightly between the right and left side of the walls and the front part has an average height of 146 mm, instead of the back part that has an average height of 210.28 mm.

To simplify the model, it was deemed appropriate to straighten the toroidal surface that faces the plasma with a toroidal length of 1290.4 mm. The side walls have also been modified by straightening a radial dimension of 554.91 mm, one of them with a 90° angle and the other with 95°. The selected radial dimension is the average dimension given by the extensions from the back part to the Tungsten layer. The total height was fixed with an increasing linear trend from a minimum of 146 mm, in the facing plasma surfaces, up to a maximum of 210.34 mm, at the end of the BZ region. These approximations for the numerical model of the FW IB apical cell geometry have been made considering the average value of the dimension length and considering a change in the volume resulting in a total power variation lower than 1%. For this configuration, two different numerical models have been produced, with different water channels layout, both including 10 square channels arranged along the poloidal direction. The difference between the two layout concerns the approach to the channels modeling, in particular as regards the channel pitch: the first layout of the IB apical cell has been designed to keep the pipe spacing constant in the whole system, that is 7.6 mm; in the second channels layout the pitch is poloidally uniform, but it varies with the radial dimension following the shape of the FW; therefore the channel pitch varies from the minimum value of 7.6 mm at the facing plasma surface, to the maximum value of 14.034 mm at the end of the BZ. The numerical models are shown in Fig. 5.

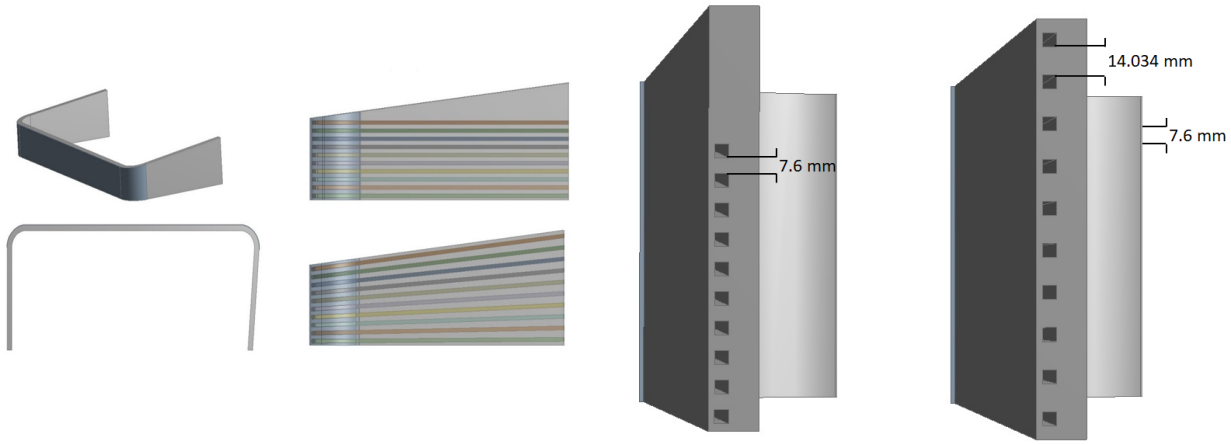

a) Isometric view of the IB apical model with different channels orientation

b) Channels pitch variation detail

Fig. 5: WCLL FW system IB apical model with different pitch of the channels

3. DEMO Thermal loads

The DEMO power plant is based on five operational phases, divided in: dwell, where the central solenoid is charging and the power is assumed at 1% of the nominal power; ramp-up, where the plasma starts to grows up his temperature and reaches the nominal power; flat-top, phase in which the plasma has reached the stationary condition and the reactor is at full power burning the fuel; ramp-down, is the opposite of the ramp-up where the plasma current returns to the initial condition; dwell phase where the central solenoid starts to recharge for another cycle [8].

The thermal loads in the WCLL BB are mainly caused by multiple sources: the neutron and charged particles fluxes generated by the fusion reaction and the thermal radiation that arise from the plasma; they can be assumed constant in the steady-state analyses, that in this work represents the full power operating phase. These phenomena can be represented by a volumetric power density into materials caused by the interaction with neutrons and a heat flux applied to the Tungsten armor, that is composed of thermal radiation and charged particles. In the present work, the mutual interaction between FW and BZ has been neglected; this assumption allows to isolate the systems and actually analyze the FW as an independent cooling system optimizing the number of water channels.

Due to the structural asymmetry of the fusion reactor, the overall heat load in the three analyzed locations is not identical, and both power contribution varies significantly along the poloidal direction. Each analyzed system has its own power curves for volumetric power and heat flux depending on the poloidal position in which they are located.

According to Ref. [9], each cell under analysis has its own power curve, that radially decreases moving from the Tungsten armor to the backplate. Regarding the equatorial IB and COB systems, the nuclear heating data are reported in

[9]; instead, for the apical IB system it was necessary, in order to obtain a correct power density, to scale the power deposition curve with the Neutron Wall Load (NWL). The load on the armor, in fact, is mainly produced by neutrons, while gamma rays have a small impact; therefore, the NWL represents well the trend of volumetric power density in the poloidal direction.

The heat flux poloidal variation is described in Refs. [10] [11] and the proper combination of the two thermal contributions, volumetric power deposition and heat flux, applied to the numerical models described in this study has been inferred by the results presented in Refs [9][10] and [11]. In fact, the volumetric power density refers to a BB numerical model divided into 7 IB modules and 7 COB modules [9]; moreover, the thermal loads related to the heat flux were obtained by a numerical model of the BB that is divided into 30 modules, 12 of IB and 18 of COB [10][11]. As mentioned above, the analysis is focused on the two equatorial cells, IB and COB where there is the maximum power deposition but a low heat flux, and one IB apical cell, with the maximum heat flux but a low volumetric power deposition. The two reference models are shown in Fig. 6: the equatorial COB cell corresponds to O4 and m23, the equatorial IB cell corresponds to I3 and m2 and the apical IB cell corresponds to I7 and m8. In Table 1 the three different systems analyzed with the relative maximum heat flux and maximum volumetric deposited power are summarized.

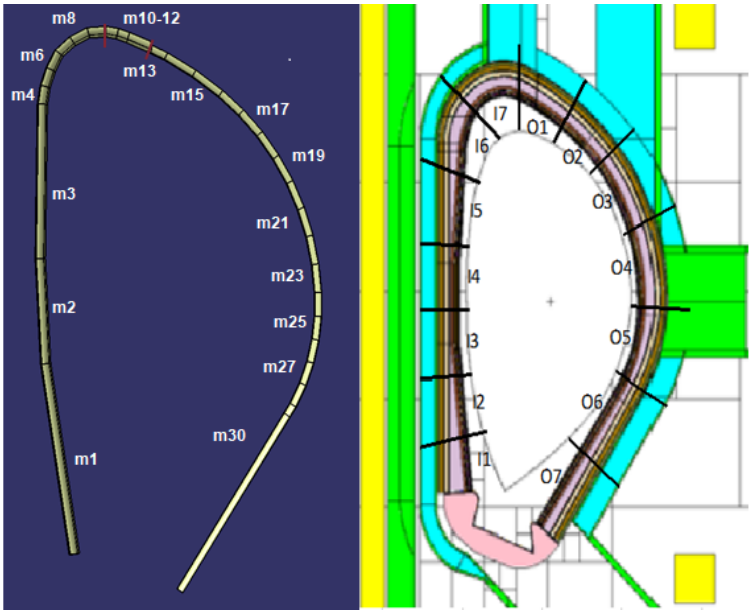

Fig. 6: Comparison between the BB models for heat flux (left, [11]) and volumetric power deposition (right, [9])

Table 1: Maximum heat flux and deposited power divided by analyzed model

System	HF module	Q^3 module	HF_{max} [MW/m^2]			Q^3_{max} [MW/m^3]
			Charged Particles [MW/m^2]	Radiation Transfer [MW/m^2]	Total [MW/m^2]	
1	m23	O4	*0.06*	*0.26*	0.32	26.77
2	m2	I3	*0.00*	*0.19*	0.19	23.38
3	m8	I7	*1.09*	*0.18*	1.27	17.30

4. Problem formulation and numerical models

To evaluate the thermal-hydraulics performance of the FW cooling system, verifying the reliability to deliver the coolant at the design temperature of 328°C to the PHTS, and to optimize the number of the water channels not exceeding the imposed Eurofer temperature limit of 550°C, different models of the FW system have been set up for the CFD analysis. The 3D finite volume models have been reproduced according to Sects. 2.1, 2.2 and 2.3, using ANSYS CFX v18.2 code, to realistically reproduce the geometry and flow features of WCLL FW cooling system and to obtain a complete and detailed temperature distribution both in the fluid (i.e. water coolant) and the solid domains (i.e. FW and Tungsten layer). For each configuration, thermal-hydraulic steady-state analyses to assess the coolant systems efficiency by removing the total power, as well as sensitivity analyses to reduce the number of water channels, have been performed. A thermal-hydraulic transient analysis has been performed for the simplified geometry of the COB equatorial cell only, named

COB*, with 2 channels referred to the layout with 4 channels, to study the behavior of the FW subjected to the pulsed operation, by referring to the transition between the dwell and the pulse phases (i.e. the Ramp Up phase). This analysis has been performed to verify if the WCLL COB FW system with 4 channels satisfies the DEMO design criteria and guarantees the required thermodynamic conditions of water in this operational phase.

The thermophysical properties of water coolant, Eurofer and Tungsten have been implemented in the commercial code with a constant value or temperature-dependent function using a polynomial fitting of data Refs. [12] and [13]. The properties of Eurofer and Tungsten have been specified in terms of density, specific heat and thermal conductivity, while water also requires the dynamic viscosity, as summarized in Table 2, Table 3 and Table 4.

Table 2: Tungsten thermo-physical properties (T in K) [12]

Value	Unit
$\rho = 19300$	kg/m^3
$c_p = 145$	J/(kg K)
$\lambda = 125$	W/(m K)

Table 3: Eurofer thermo-physical properties (T in K) [12]

Equation	Unit
$\rho = 7874.3 - 0.361 \cdot T$	kg/m^3
$c_p = -438.83 + 4.9838 \cdot T - 8.7371 \cdot 10^{-3} \cdot T^2 + 5.3333 \cdot 10^{-6} \cdot T^3$	J/(kg K)
$\lambda = 60.915 - 9.081 \cdot 10^{-2} \cdot T + 6.5 \cdot 10^{-5} \cdot T^2$	W/(m K)

Table 4: Water thermo-physical properties (T in K) [13]

Equation	Unit
$\rho = -1.4226 \cdot 10^{-2} \cdot T^2 + 14.122 \cdot T - 2693$	kg/m^3
$c_p = 9.8485 \cdot 10^{-3} \cdot T^3 - 16.39861 \cdot T^2 + 9118.681 \cdot T - 1.6882247 \cdot 10^6$	J/(kg K)
$\lambda = -1.2024 \cdot 10^{-5} \cdot T^2 + 1.1846 \cdot 10^{-2} \cdot T - 2.2804$	W/(m K)
$\mu_d = (-8.095238 \cdot 10^{-4} \cdot T^2 + 0.5722429 \cdot T + 29.67213) \cdot 10^{-6}$	kg/(m s)

To simulate the power deposition on WCLL FW systems, two main thermal loads have been imposed for the analyses: the heat flux on the Tungsten layer that faces the plasma, and the volumetric power density on the entire FW volume. A maximum nominal heat flux on the COB, IB and apical IB of 0.32, 0.19 and 1.27 MW/m^2, respectively, composed by charged particles and thermal radiation has been imposed onto the armor straight surface Ref. [11]. Concerning the elbows, a decreasing linear trend equation with the radial direction has been implemented, this to account the decreasing value of the normal component of the heat flux due to the variation of the incidence angle, $q''_{SW} = \left[1 - \frac{(y_0 - y)}{y_{tot}}\right] \cdot q''_{max}$.

Regarding the volumetric power deposition, three different curves, depending on the radial direction, have been implemented in CFX, one per each model according to the poloidal position of the cell, using the data from Ref. [9]. To realistically reproduce the radial power deposition trend into solid structures, multiple curves have been created to obtain an appropriate power deposition in each system since, in each analyzed model, the total deposited power is variable in accordance with the poloidal position in the reactor, overall geometric dimension and number of FW channels.

For each steady-state analyses, the reference water thermodynamic cycle is assumed as in the WCLL BB 2017 design [12][14][15]. The cycle, still based on PWR conditions, foresees water coolant entering at 295°C and exiting at 328°C, at 15.5 MPa. The imposed water mass flow rate varies in each run and it is evaluated using RELAP5/Mod3.3 [13], obtaining in all the analyses the required value for the outlet water temperature (328°C), since the total power deposited in the FW changes. The variation is because decreasing the number of channels, the amount of Eurofer in the model is greater and this leads to an increase in the volumetric deposited power.

In order to assess the WCLL behavior during a pulse phase, transient thermal loads have been considered. To simulate the power deposition during these phases, time-dependent curves have been implemented in CFX according to Ref. [16]. The analysis includes the ramp-up phase, passing from the dwell state to the pulse phase. In this analysis, a time of 90 seconds for the ignition ramp has been assumed. Heat flux and deposited power have been set with a time-dependent function during the ramp-up. The transient normalized power curves are summarized in three different phases resumed in Table 5 and shown in Fig. 7.

Table 5: WCLL Transient normalized power curves

Time interval [s]	Phase	Normalized power equation [-]
0 – 10	Dwell	$P_{norm} = 0.01$
10 – 25	Ramp Up	$P_{norm} = \left((1.3333 \cdot 10^{-5} \cdot t^3) - (5.9997 \cdot 10^{-4} \cdot t^2) + (1.2166 \cdot 10^{-2} \cdot t) - 6.4997 \cdot 10^{-2}\right)$
25 – 100	Ramp Up	$P_{norm} = \left((-1.9959 \cdot 10^{-7} \cdot t^3) + (1.3149 \cdot 10^{-4} \cdot t^2) - (1.5292 \cdot 10^{-3} \cdot t) + 3.1225 \cdot 10^{-2}\right)$
>100	Pulse	$P_{norm} = 1.0$

In addition, the inlet water temperature of the FW water also varies during the transient (Ref. [16]), to ensure proper cooling of the Eurofer structures and adequate coolant temperature at the outlet. Unlike the power curve that reaches the plateau after 100 seconds, the water coolant inlet temperature does not reach a steady value until 300 seconds after the transient starts. The FW cooling water does not follow a smooth trend; therefore different equations have been used to recreate its variation, reported in Table 6. In Fig. 8 the FW water inlet temperature versus time is shown. In this case, a constant water mass flow rate has been imposed during the whole transient and it corresponds to half of the WCLL COB FW system with 4 channels (0.27458 kg/s).

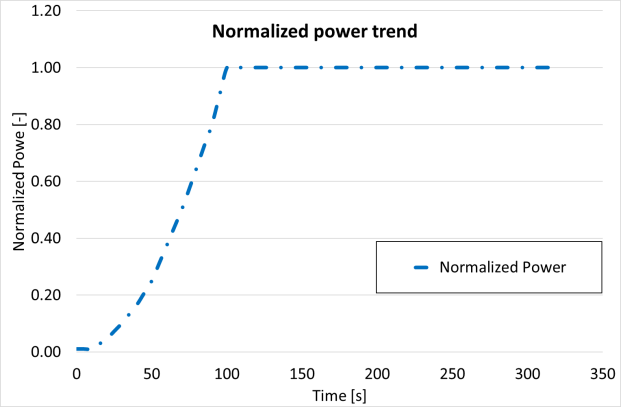

Fig. 7: WCLL transient normalized power curves ramp-up

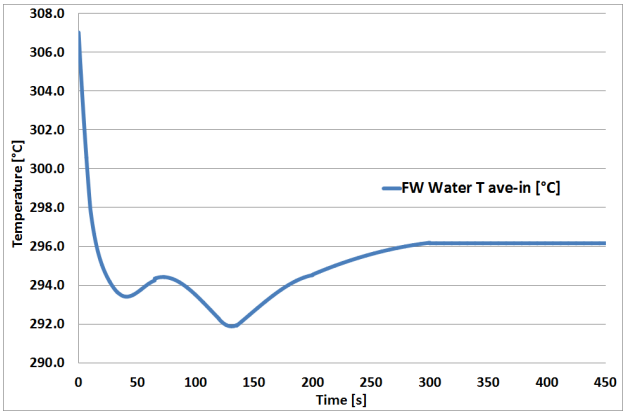

Fig. 8: WCLL FW water inlet temperature transient trend

Table 6: WCLL Transient water coolant inlet temperature curves

Time interval [s]	Inlet temperature equation [°C]
0 – 10	$T_{inlet} = \left((1.87 \cdot 10^{-2} \cdot t^2) - (1.0964 \cdot t) + 306.88\right)$
10 – 35	$T_{inlet} = \left((1.247 \cdot 10^{-5} \cdot t^4) - (1.3805 \cdot 10^{-3} \cdot t^3) + (6.0284 \cdot 10^{-2} \cdot t^2) - (1.3196 \cdot t) + 306.2119\right)$
35 – 65	$T_{inlet} = \left((5.0 \cdot 10^{-8} \cdot t^4) - (9.2061 \cdot 10^{-5} \cdot t^3) + (1.4243 \cdot 10^{-2} \cdot t^2) - (0.7171 \cdot t) + 304.9197\right)$
65 – 120	$T_{inlet} = \left((1.2230 \cdot 10^{-5} \cdot t^3) - (4.1656 \cdot 10^{-3} \cdot t^2) + (4.0968 \cdot 10^{-1} \cdot t) + 281.8016\right)$
120 – 135	$T_{inlet} = \left((1.4930 \cdot 10^{-5} \cdot t^3) - (2.3740 \cdot 10^{-3} \cdot t^2) - (1.4376 \cdot 10^{-1} \cdot t) + 317.7357\right)$

135 – 200	$T_{inlet} = \left((-4.40 \cdot 10^{-6} \cdot t^3) + (1.9146 \cdot 10^{-3} \cdot t^2) - (2.2627 \cdot 10^{-1} \cdot t) + 298.2386\right)$
200 – 300	$T_{inlet} = \left((-9.2470 \cdot 10^{-5} \cdot t^2) + (6.2590 \cdot 10^{-2} \cdot t) + 285.5766\right)$
>300	$T_{inlet} = 296.0$

The other boundary conditions adopted for all the models are:

- Periodic boundary conditions on the upper and lower surfaces of FW and Tungsten layer, in poloidal direction, to simulate the presence of adjacent FW units;
- Adiabatic condition to the back walls of FW and Tungsten;
- Mass flow rate and static pressure imposed in the fluid domain at inlet and outlet sections, respectively;
- No-slip condition at the interface between coolant and the circuit steel walls.

In order to select the appropriate CFX turbulence models, the average Reynolds number has been analytically evaluated in the range from 57000 (IB3) to 260000 (IB7), resulting in turbulent flow for all the models. The two-equations k-ω Shear Stress Transport (SST) model has been selected as an appropriate method to simulate the turbulence effects because it is able to solve the viscous sublayer explicitly with y+≤1 without losing accuracy in the free stream of the channels, as reported in Ref. [17]. Moreover, it has been applied to a large variety of similar turbulent flows (Refs. [6],[7],[12] and [15]).

A complete set of runs and boundary conditions are summarized in Table 7.

Table 7: FW parametric analysis overview and boundary conditions

Run [#]	System	Analysis Type	N° channels	Water T_{inlet} [°C]	Pitch	Water mass flow rate [kg/s]	FW HF_{max} [MW/m^2]	Total Power [kW]
1	COB	Steady	10	295.0	Constant	0.53110	0.32	102.820
2	COB	Steady	6	295.0	Constant	0.54315	0.32	105.150
3	COB	Steady	4	295.0	Constant	0.54918	0.32	106.320
4	IB	Steady	10	295.0	Constant	0.32720	0.19	63.350
5	IB	Steady	4	295.0	Constant	0.35130	0.19	68.000
6	IB_{apical}	Steady	10	295.0	Constant	1.45200	1.27	281.100
7	IB_{apical}	Steady	10	295.0	Variable	1.45200	1.27	281.100
8	COB*	Transient	2	306.9	Constant	0.27458	0.32	53.160

5. Mesh independence analysis

For the two calculations, steady-state and transient, a mesh independence study has been performed, allowing accurate results and reasonable calculation time, using meshes with different degree of detail. All the geometrical models are developed as a single part, to simulate the heat transfer between the multiple components, solids and fluid using a conformal mesh. Hexahedral and tetrahedral elements were adopted in the models, considering the geometrical features of the domains, many and different local controls are inserted to properly define the complex geometry. For this purpose, different code tools were exploited, such as: sizing control, sweep method, mapped face, and the inflation control near the solid walls for the resolution of the viscous sub-layer (y^+=1) of the water, based on a maximum velocity of 7 m/s.

The analysis was conducted to establish the independence of results from the grid and to optimize the number of elements of the model. The simulations have been carried out with a reduced model of the COB FW, because the periodic geometry allowed to carry out the analysis on a fifth of the entire model, taking into consideration only two channels in counter current. Four meshes (A, B, C and D), with an increasing degree of detail, were considered. The analyses have been performed with the above-mentioned boundary conditions and a water mass flow rate set to 0.10622 kg/s. The performed calculation are summarized in Table 8, and the related results are shown in Fig. 9.

Table 8: Steady-state mesh independence analyses

Mesh	Elements	T_{out} Water [°C]	T_{max} Eurofer [°C]	T_{max} Tungsten [°C]
A	0.71M	326.50	389.78	396.09

B	1.56M	327.42	392.91	397.86
C	3.87M	327.48	393.89	398.90
D	6.21M	327.48	393.96	398.92

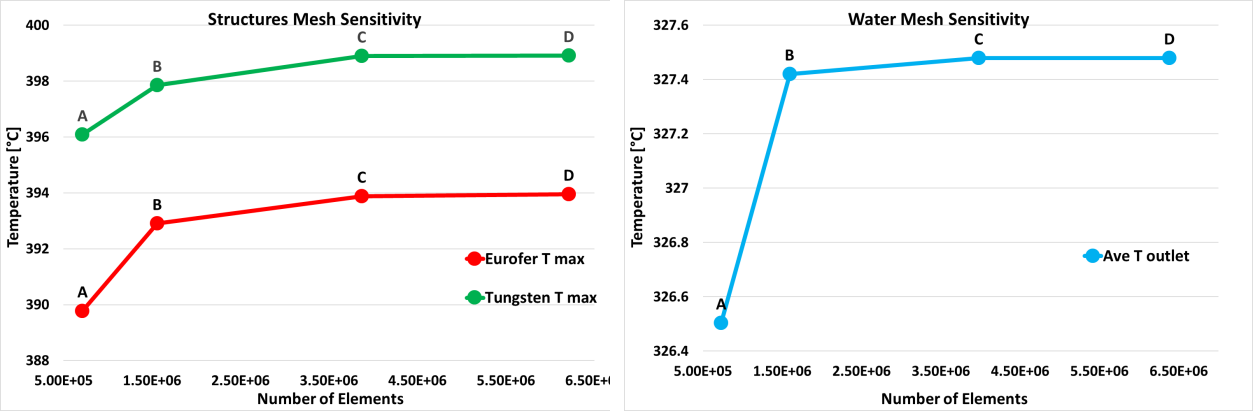

a) Structures mesh sensitivity b) Water mesh sensitivity

Fig. 9: Steady-state FW system mesh independence results

The results show that the finer mesh (D) does not provide significant improvements compared with mesh C; therefore this last is adopted to have reasonable computational costs.

Regarding the transient analysis, a slightly modified version of the mesh used for the steady state analysis has been used to reduce the computational costs. Since the objective of this analysis is not to acquire extremely accurate values at local level but, rather, to investigate the global performance of the cooling system during a reactor operational phase, it has been deemed acceptable to reduce degrees of accuracy in favor of the stated goal. Two mesh sensitivity studies have been carried out, the first one focused on the solid domain resolution and the other one on the water wall treatment.

For the former study, the number of axial divisions (Fig. 10) of the structures has been varied, checking the final temperature of the structures. Regarding the fluid domain of the water, a y^+=1 calculated on a velocity of 5 m/s has been imposed, to fully resolve the sub-viscous layer. The analyses of this first mesh independence study are summarized in Table 9, and the related results are shown in Fig. 11. As reported, the mesh refinement of the solid structures does not produce significant result variation changing from mesh (A) to (D). The heat transfer coefficient is the only quantity that shows an appreciable variation, approximately 3.6% from mesh (A) to mesh (D). Considering that the model was set, in the fluid domain, with y^+=1 to fully resolve the viscous sub-layer, it has been assessed to further analyze the mesh (A) by varying the y^+.

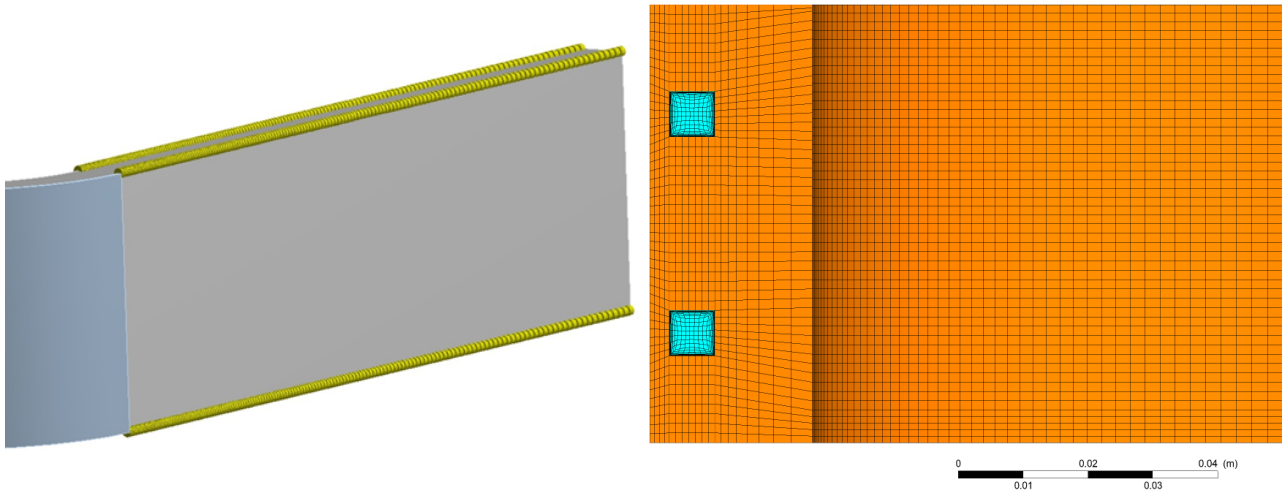

a) Axial edge sizing b) Eurofer and water mesh detail

Fig. 10: FW COB* mesh detail

The second mesh sensitivity was carried out by varying the control of the y^+ from 1 up to 20, based on a velocity of 5 m/s. The performed analyses and the related results are reported in Table 10. In this case, the mesh (A1) is the finer mesh, corresponding to the mesh (A) of the previous case, and the coarser mesh is (A4) with y^+=20, achieving a 10%, 17% and 20% in reduction of elements, respectively. The table shows that the meshes (A3) and (A4) feature unacceptable deteriorations for the HTC estimate accuracy. The mesh (A2) has been selected as the reference mesh, since it allows the best compromise between computational time and accuracy.

Table 9: Transient mesh optimization analyses with fixed y^+=1

Mesh	Elements	Average Skewness	Average Orthogonal Quality	y^+	FW T_{max} [°C]	Tungsten T_{max} [°C]	Water $T_{out-ave}$ [°C]	P Drop [kPa]	HTC [W/m² K]
A	0.54M	0.233	0.701	1	466.70	470.70	327.63	32.235	30741
B	0.87M	0.218	0.719	1	466.00	470.09	327.73	32.032	31311
C	1.42M	0.199	0.768	1	465.56	469.69	327.80	31.889	31656
D	2.49M	0.189	0.785	1	465.29	469.45	327.84	31.787	31890

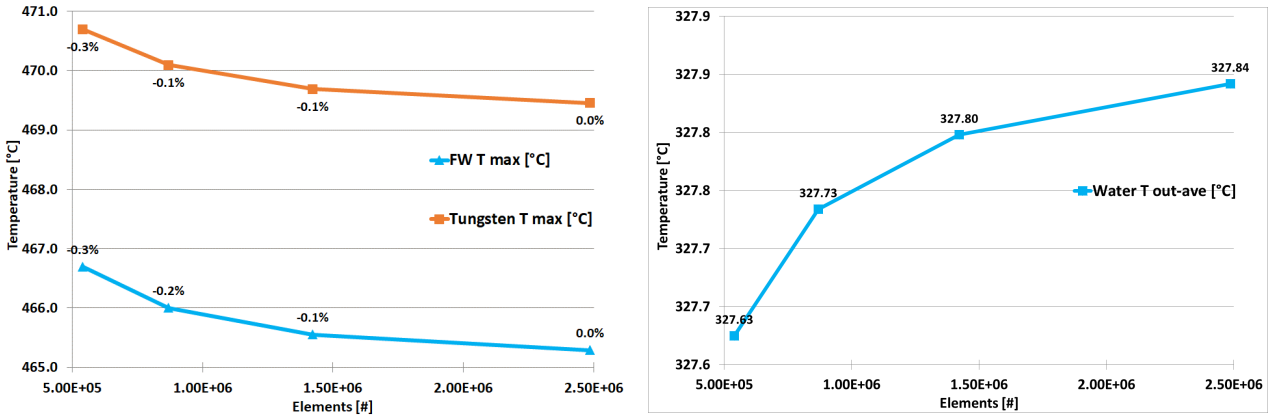

a) Structures domain mesh sensitivity b) Water domain mesh sensitivity

Fig. 11: Transient FW system mesh optimization results

Table 10: Transient mesh optimization analyses with variable y^+

Mesh	Elements	Skeweness	Orthogonal Quality	y^+	Water $T_{out-ave}$ [°C]	P Drop [kPa]	HTC [W/m² K]	Var T Water	Var P Drop	Var HTC
A4	0.43M	0.209	0.833	20	327.63	33.597	10360	0.0%	4.2%	66.3%
A3	0.45M	0.210	0.803	10	327.63	33.295	21980	0.0%	3.3%	28.5%
A2	0.46M	0.225	0.769	5	327.63	32.153	31633	0.0%	0.3%	2.9%
A1	0.54M	0.233	0.701	1	327.63	32.235	30741	0.0%	0.0%	0.0%

6. Results and discussion

The results of eight runs performed are discussed below. They differ in terms of: the FW number of channels, concerning the IB apical cell the geometry, and imposed boundary conditions. The first seven runs have been performed in steady-state conditions to optimize the channels layout. The last run has been performed in transient conditions, to obtain a temperature trend during the pulsed phase of DEMO, precisely the ramp-up phase.

The relevant parameters of the steady-state runs are reported in Table 11, where the optimized configuration of each model (i.e. COB, IB and IB apical cell) satisfied the Eurofer temperature requirement and adequate water condition for the PHTS, and in Fig. 12 is reported the maximum temperature trend for Tungsten and Eurofer FW chase, as the number of channels changes in runs from #1 to #5, and the geometry of channels varies in runs #6 and #7. The obtained results are hereafter discussed, divided by models and type of run.

Table 11: Steady-state: main output parameters

Parameters	Value							Unit
	COB Equat.			IB Equat		IB Apical		
Run	#1	#2	#3	#4	#5	#6	#7	-
N° Channels	10	6	4	10	4	10	10	#
Tungsten T max	398.9	418.2	468.0	388.1	452.1	570.5	567.6	°C
FW T max	393.8	413.7	463.9	385.2	449.8	552.3	548.6	°C
Water T ave-out	327.7	327.8	327.8	327.8	328.0	327.7	328.3	°C
Water T max	357.9	360.7	364.8	359.2	367.8	398.5	397.8	°C
Water v ave-out	1.651	2.815	4.269	1.023	2.747	4.514	4.535	m/s
Water v ave	1.581	2.671	4.038	0.979	2.597	4.281	4.293	m/s
Water v max	2.006	3.362	5.050	1.254	3.275	5.376	5.394	m/s
Water Pressure Drop	5.85	15.097	31.898	1.79	10.35	33.28	33.50	kPa
Fr Number	48.5	140.7	323.6	18.4	132.5	362.0	362.0	-
Re Number out	93300	159000	241000	57700	156000	255000	256000	-
CHF	2.25	2.66	3.15	2.13	2.97	3.65	3.65	MW/m²
Channel HF max	0.596	0.793	1.10	0.46	0.88	2.18	2.14	MW/m²

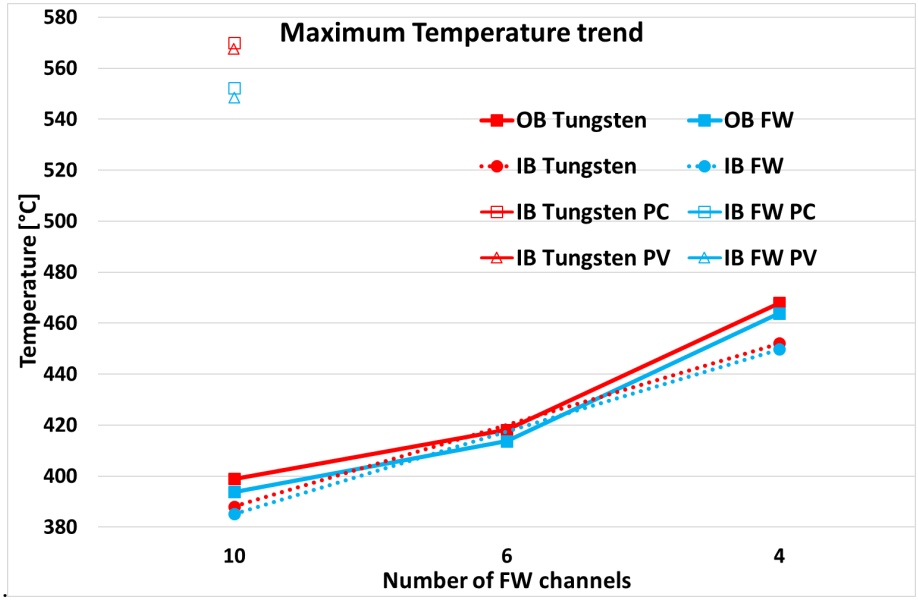

Fig. 12: WCLL FW optimization analyses: structures maximum temperature comparison

6.1. FW OB results

Regarding the OB equatorial elementary cell, three configurations have been investigated: run#1, #2 and #3, with 10, 6 and 4 channels, respectively. Considering all the runs, as expected, the water outlet temperatures, obtained from the CFD-Post as the temperature averaged on the mass flow rate and the overall outlet tube sections, are very similar: 327.7°C, 327.8°C and 327.8°C, respectively. The pressure drops increases as the number of channels present in the FW decreases, going from 5.85 kPa of run #1, to 15.097 kPa of run #2 and up to 31.898 kPa of the run #3. This marked variation is also because the average water velocity increases from 1.58 m/s, 2.67 m/s and 4.04 m/s, respectively. This increase in pressure drops can be considered negligible, compared with the pressure drops of the entire FW circuit, as demonstrated in [18]. Analyzing the maximum water temperature, it exceeds the saturation temperature (344.8°C at 15.5 MPa), which should result in a local boiling but, in the CFX numerical model, the phase change is not considered. The possibility of thermal crisis occurrence has been then evaluated. For horizontal tubes and high flow rates, according to Ref. [19], the Critical

Heat Flux (CHF) can be predicted using the correlation $q''_{CHF,Hor} = k * q''_{CHF,Ver}$. The parameter k varies with the Froude number $Fr = {G^2}/{(\rho_L^2 g D)}$, where G is the total mass flux (kg/m² s), ρ_L is the density of the saturated liquid at 15.5 MPa (kg/m³), g is the gravity acceleration (m/s²) and D corresponds to the diameter of the tube (m); q''$_{CHF,Ver}$ is the correlation for the vertical channels subjected to the same heat flux. The value of k is calculated in term of Fr number as $k = 0.725 * Fr^{0.082} \leq 1$. Thus, if k is greater than 1, k=1 is adopted and also k=1 at Fr number greater than 50. Regarding the three cases, Fr = 48.5, 140.7 and 323.6 are obtained, thus is imposed k=0.996 for the first case, and k=1 for the remaining two cases. The Tong's correlation [20] has been adopted to evaluate the q''$_{CHF,Ver}$, obtaining q''$_{CHF,Hor}$ = 2.25 MW/m², 2.66 MW/m² and 3.15 MW/m² for 10, 6 and 4 channels layout. The portion of the FW channels affected by the highest HF is the front-toroidal part of the channels, in which the maximum HFs are 0.596 MW/m², 0.793 MW/m² and 1.1 MW/m², respectively. Therefore, no thermal crisis within the FW channels occurs, but it is likely that limited areas of the channel wall can exist where subcooled nucleate boiling is the dominant heat transfer regime.

Regarding the structural materials, all the three runs return a symmetrical temperature field both in toroidal and poloidal direction, due to the counter current flow and the poloidal periodicity. The three configurations result below the required limits of 1300°C for the Tungsten and 550°C for the FW. Reducing the number of channels, the maximum temperature in the Eurofer increases from the value of the reference layout (393.6°C) by 20.1 degrees for 6 channels and 70.3 degrees for 4 channels. The run #3 with 4 channels returns a maximum temperature of 463.9°C that is around 86 degrees below the imposed limit. Regarding the Tungsten domain, with the reduction of the channel number, it follows the same temperature trend as the Eurofer, increasing by 19.5 degrees from 10 (398.7°C) to 6 and 69.3 degrees from 10 to 4, and in case #3 returns a maximum temperature of 468°C, widely below the limit. In Fig. 13 the characteristic temperature field of the FW Eurofer structures with 4 channels and a radial-poloidal cut at the middle of the FW toroidal length is presented. The results summarized in Table 11 show that the configuration with 4 water channels returns Eurofer and Tungsten structures not exceeding the temperature limits, enhanced water performances ensuring outlet water conditions suitable for the PHTS and a reduction of the amount of water in the first centimeters of the elementary cell, that positively influences the TBR.

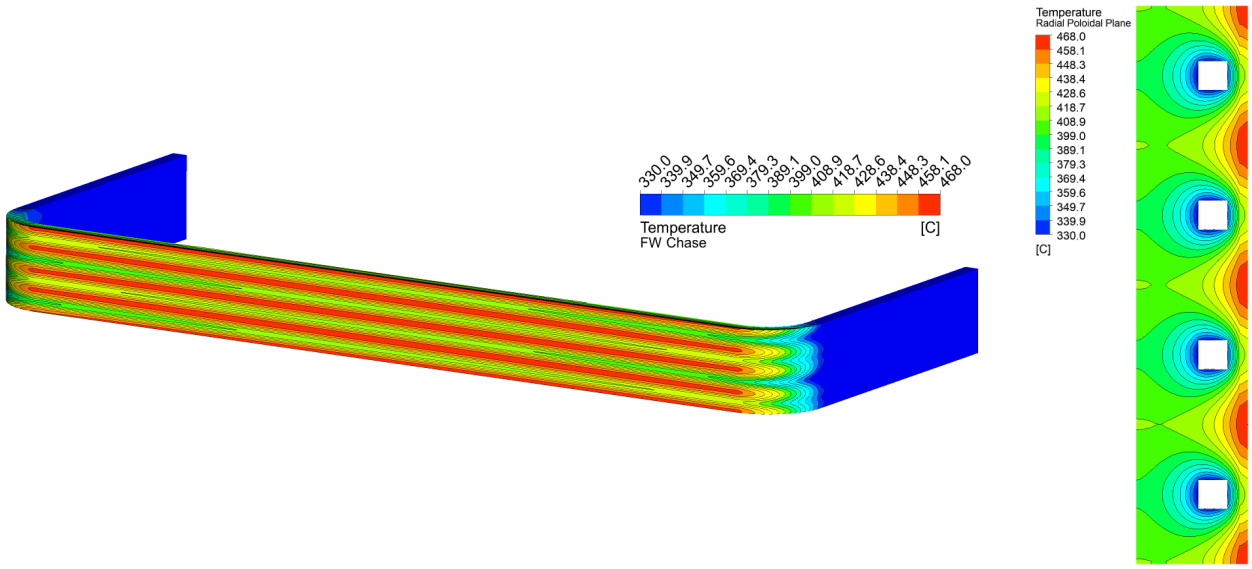

a) FW domain temperature contour

b) Radial-poloidal plane temperature contour

Fig. 13: WCLL FW COB equatorial cell with 4 channels temperature contours

6.2. FW IB results

Regarding the IB equatorial elementary cell, two different runs have been performed, run #4 and #5 with 10 and 4 FW water channels, respectively. As expected, the average outlet temperature in both cases is 327.8 and 328°C, concerning the maximum water temperature, it reaches 359.2 and 367.8 °C. The CHF has been evaluated with the same correlation used in the FW COB analysis, in terms of k and Fr number. Thus, for the run #4 k = 0.92, and for run #5 k = 1, due to Fr = 18.4 and 132.5, respectively. The CHF is evaluated, like in the previous cases, obtaining 2.13 and 2.97 MW/m², values to be compared with actual ones 4.6 and 3.4 times lower in the two configurations, respectively. Therefore, the optimized case with 4 channels has a good margin to avoid the thermal crisis. As the number of channels

decreases, the pressure drops increases about 6 times, and the average velocity rises 2.65 times, optimizing the cooling performance in terms of HTC. Even in this case, the increase of the pressure drops is negligible, as mentioned in Section 6.1 and in Ref. [18], having an order of magnitude of 10 kPa.

Concerning the FW solid domain, the standard configuration returns temperatures more than 150 degrees below the required Eurofer limit, and the optimized one (4 channels) about 100 degrees below that limit. This is due to the low HF imposed on the Tungsten layer compared to the COB. The Tungsten domain returns temperatures 3 degrees higher than the value obtained in the FW domain. The structures temperature field is symmetrical in toroidal and poloidal directions in both runs. In Fig. 14 the Eurofer temperature distribution of the optimized configuration is shown, with a focus on the radial poloidal plane of the solid structure domains placed at the mid toroidal length of the facing plasma surface. Also in this case, the optimized configuration guarantees proper refrigeration of the structures with a water volume reduction and optimal water conditions to deliver to the PHTS.

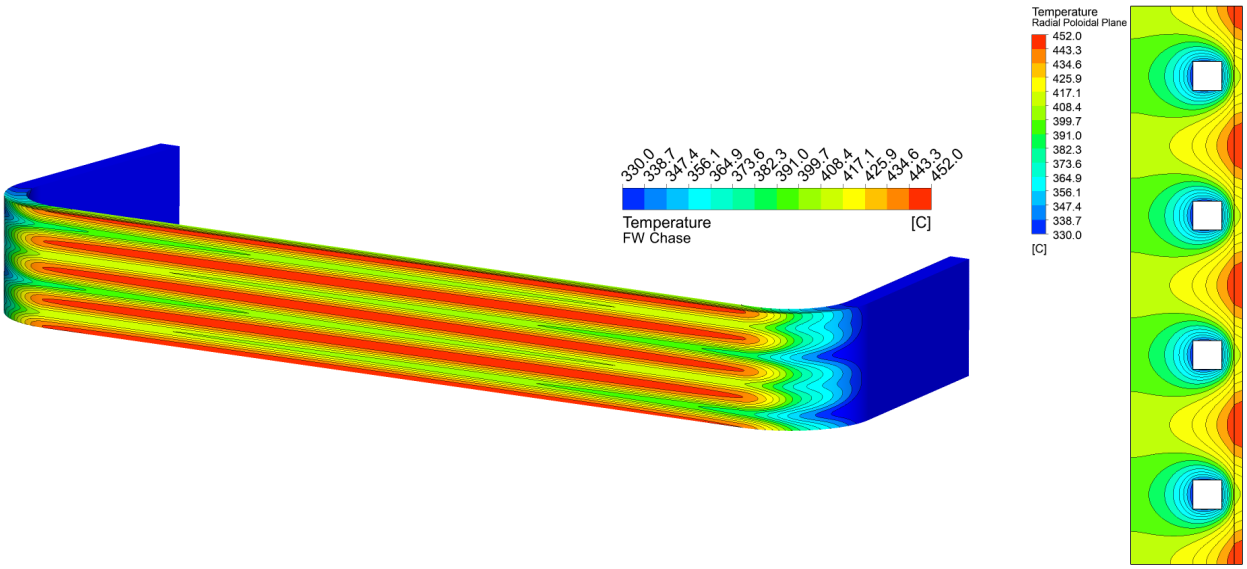

a) FW domain temperature contour

b) Radial-poloidal plane temperature contour

Fig. 14: WCLL FW IB equatorial cell with 4 channels temperature contours

6.3. FW IB apical results

The IB apical elementary cell is subjected to the highest HF on the Tungsten layer. Two different calculations have been performed, run #6 and #7, both with 10 FW water channels but with a different orientation of the channels; the first one with a constant poloidal pitch and the second case with a variable poloidal pitch along the radial length. As in the previous cases, the water mass flow rate was preliminarily evaluated to obtain the outlet conditions close to the design PHTS criteria (328°C) resulting 327.7 and 328.3, respectively for #6 and #7. The maximum temperature of the water reaches higher values than in the previous five cases, exceeding by about 50 degrees the saturation temperature of the water at 15.5 MPa. In these two cases, the Fr number reaches the highest value of 362, due to the high mass flow rate required to accommodate the highest HF on the Tungsten layer. The CHF is 3.65 MW/m^2 in both cases and, despite it is the highest value in all the analyzed configurations, the margin to the thermal crisis is reduced as the actual heat flux is only 40% lower than the CHF value, resulting in a region of interest for further assessments with more detailed analyses.

Evaluating the FW domain, the run #6 returns a Eurofer temperature that exceeds the required limit by 2.3 degrees. The hot spot is located in the upper part of the straight toroidal surface of the FW (Fig. 15 (a)). The run #7 instead, returns a maximum temperature 1.4 degrees below the limit (Fig. 15 (b)). Both cases show that the poloidal and radial thermal fields are not symmetrical.

To evaluate the temperature distribution, three different radial-poloidal cuts are reported in Fig. 16, two of which for the case #6, one in the middle toroidal length and the second in correspondence with the hot spot region; the third cut is in the middle of the toroidal length of the case #7. As reported, due to the variation in the poloidal height of the cell, in run #6 (Fig. 16 (a)-(b)) there is a periodicity of the isotherms in the toroidal centerline, but not on the elbow, due to a non-regular geometry, this means that the channel does not properly refrigerate the structure, generating a hot spot. In run #7

(Fig. 16 (c)) these effects do not arise, returning a warmer temperature field at the bottom part of the FW, but below the required Eurofer limit.

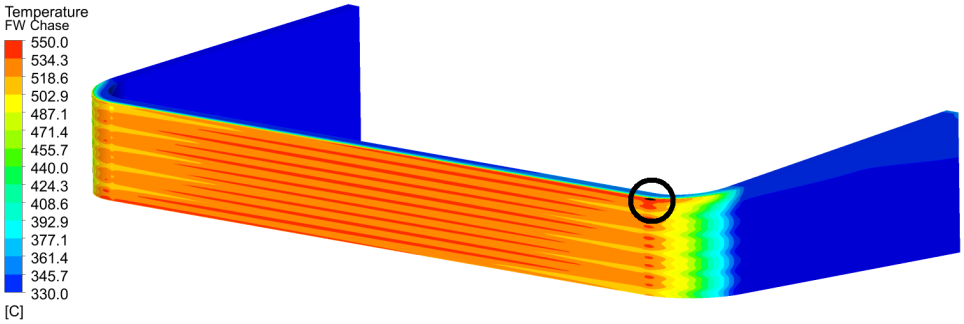

a) WCLL IB apical cell Eurofer FW domain with water channels with constant pitch

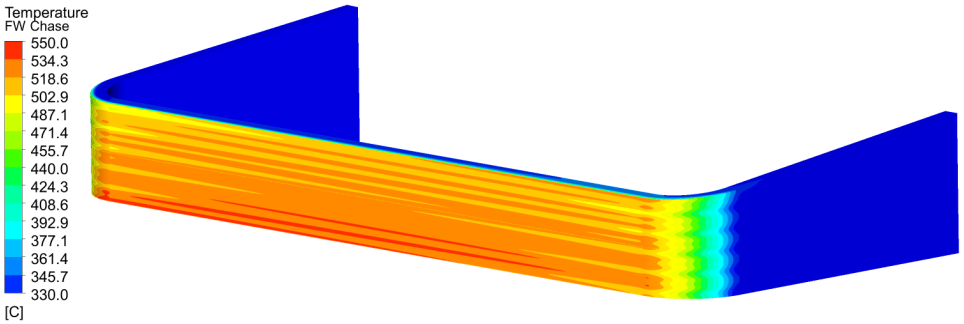

b) WCLL IB apical cell Eurofer FW domain with water channels with variable pitch

Fig. 15: WCLL FW IB apical cell Eurofer temperature contours comparison

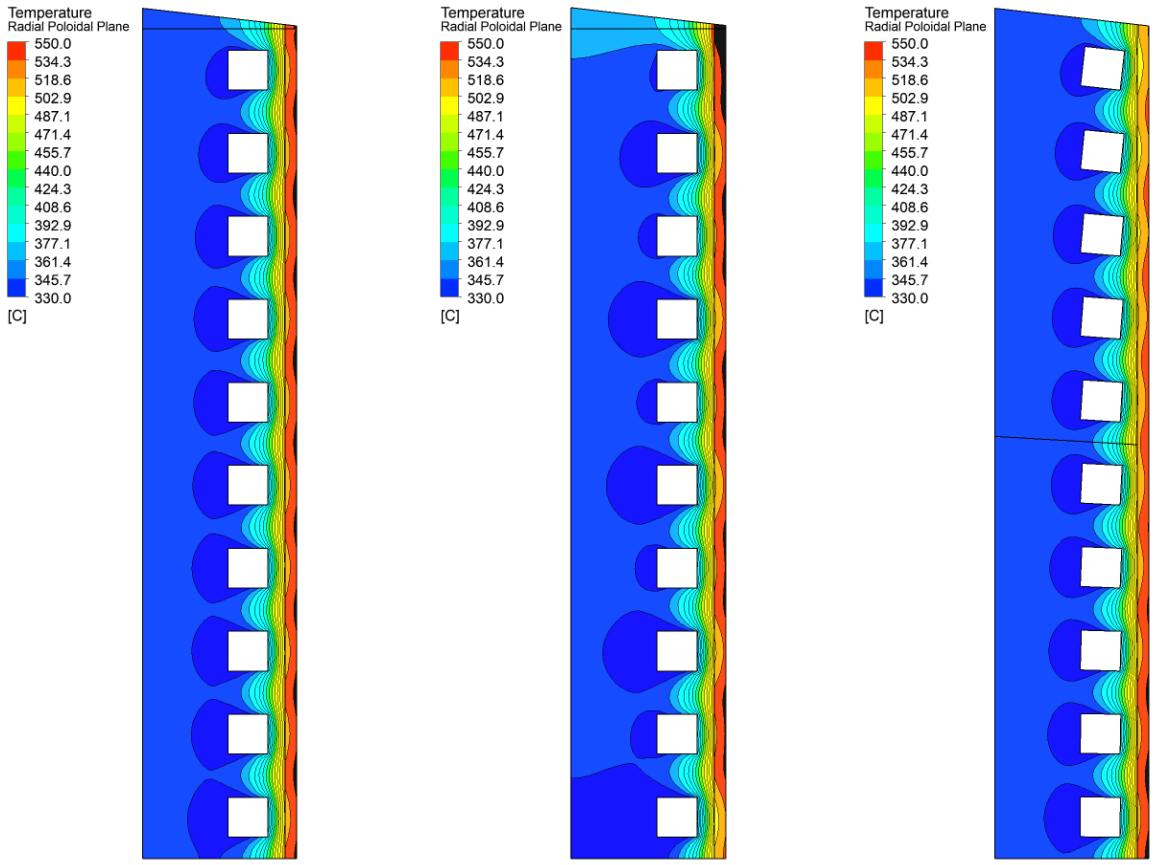

a) Constant pitch midplane b) Constant pitch hot spot plane c) Variable pitch midplane

Fig. 16: WCLL FW IB apical cell different radial-poloidal temperature contours (black region T > 550°C)

6.4. FW OB Transient results

The transient analysis of the COB FW system with 4 channels has been performed referring to half geometry, due to the poloidal periodicity of the system. As discussed above, the geometry and the obtained results allow to modify the model, reducing it to an elementary geometry composed by 2 counter current water channels and a structure having half of the total height of the elementary system. This analysis recreates the pulse-dwell phase, starting from the dwell phase, where the total power is 1% of the nominal power. The analysis has been carried out to evaluate the Eurofer thermal field and the water outlet conditions of the FW system during the transient.

The simulation has been performed for a total time of 450 s, to guarantee adequate steady conditions at its end, recreating the pulsed phase. The total duration of the transient also provides the timing within which the reactor returns effectively to normal operation in steady-state conditions. In Fig. 17 the steady initial condition of the dwell phase have been reported; it shown that the Eurofer domain returns a symmetrical and refrigerated temperature field and the radial-poloidal plane shows that the periodicity of the channels reflects the results previously obtained.

Regarding the transient phase, the maximum temperatures evolution for Tungsten and Eurofer domains during the whole transient have been reported in Fig. 18. The structures do not exceed the required limits and those results are comparable with the results summarized in Table 11, confirming that the system returned to a steady-state condition in normal operation. It can be seen from the figure that the structures maximum temperature comes to a condition of stationarity after 300 s, after the time where the water inlet temperature has reached a constant value.

Another interesting parameter is the time within which the FW outlet water returns to suitable temperature values for the PHTS. Analyzing Fig. 19, it can be noted that after 200 s the water overcomes 325°C, starting to stabilize around 328°C, and a steady outlet temperature condition is obtained after 300 s. As shown in the previous cases the maximum water temperature exceeds the saturation temperature and since the inlet temperature water varies during the transient and the CHF varies according to the subcooling degree, it is necessary to evaluate this last during the transient. As reported in Fig. 20, there is no thermal crisis during the transient and the maximum HF in the channel increases in the first 100 seconds with a parabolic trend that recalls the imposed normalized power evolution.

In Table 12 the main global parameters of the transient simulation at the end (450 s) are reported.

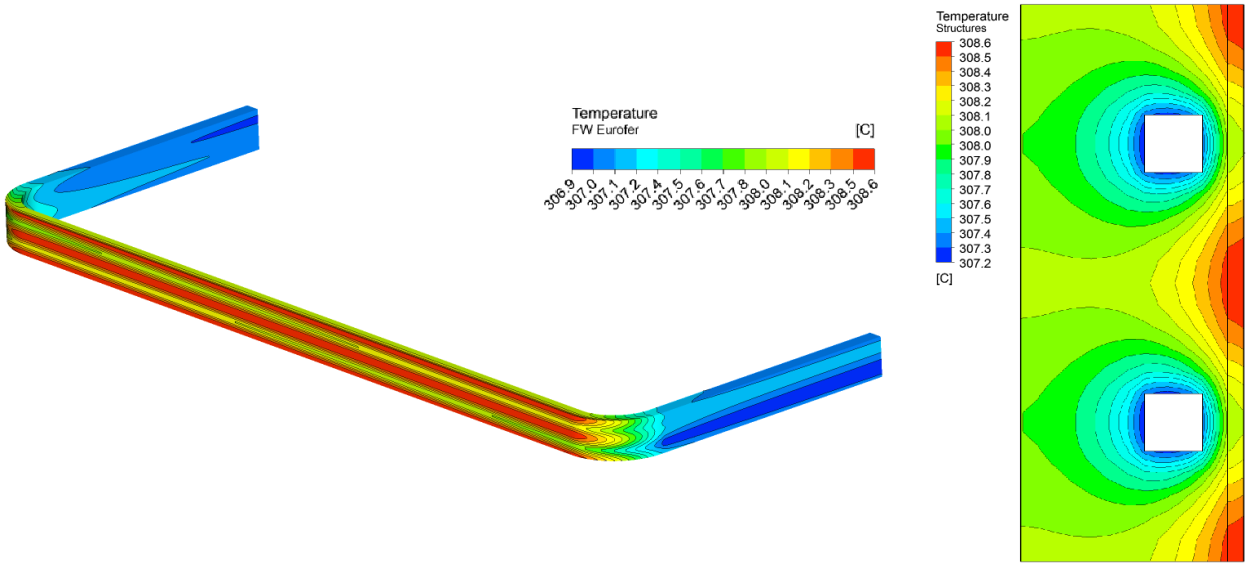

a) FW Eurofer domain temperature contour

b) FW radial poloidal plane temperature contour

Fig. 17: FW Transient different temperature contour of the dwell initial condition

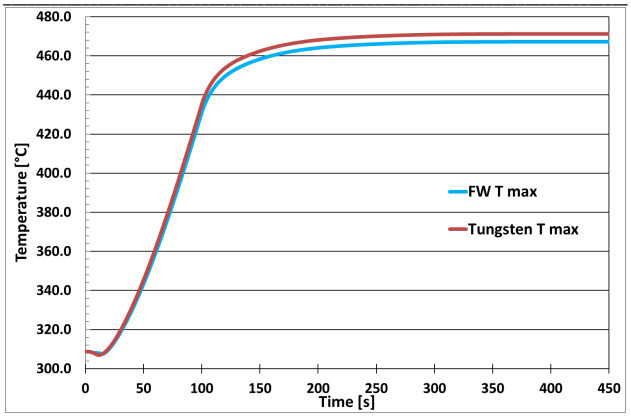

Fig. 18: FW Transient maximum temperature of the structures trend during the whole transient

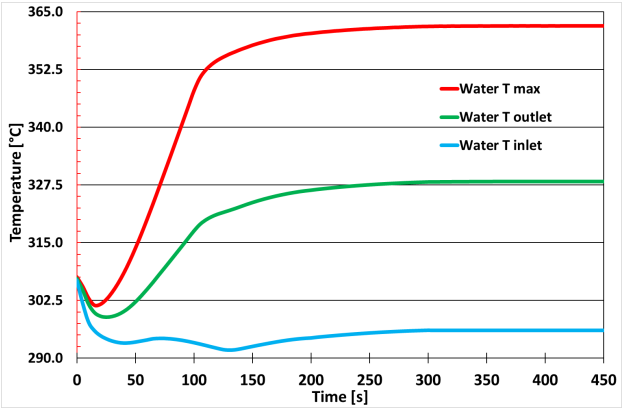

Fig. 19: FW Transient average water outlet temperature trend during the whole transient

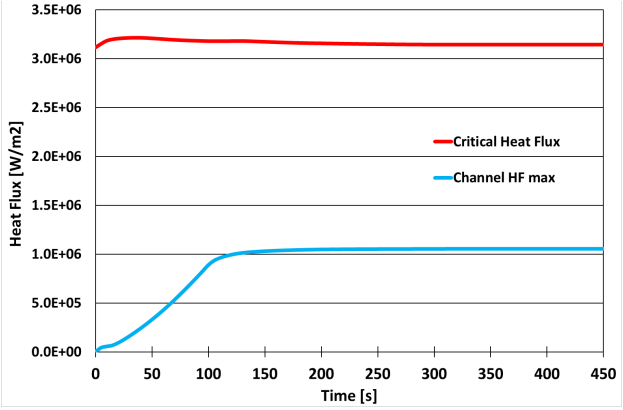

Fig. 20: FW Transient CHF and maximum heat flux comparison during the whole transient

Table 12: FW Transient relevant results at steady-state conditions (@ 450 s)

Parameters	Value	Unit
Tungsten T max	471.2	°C
FW T max	467.2	°C
Water T ave-in	296.2	°C
Water T ave-out	328.4	°C
Water T max	362.0	°C
Water v ave-in	3.795	m/s
Water v ave-out	4.281	m/s

7. Conclusions

The cooling performance of the WCLL BB FW has been investigated using a CFD approach. The analyses, based on the WCLL 2018 design, focused on three different positions: the equatorial cell of the central outboard segment, subjected to the maximum outboard volumetric deposited power and low heat flux; the equatorial cell of the inboard segment, subjected to the maximum inboard volumetric deposited power and low heat flux; and the apical cell of the inboard segment, subjected to a low volumetric deposited power and the highest inboard heat flux. A computational thermal and fluid-dynamic models of these FW systems have been developed using the commercial CFD code ANSYS CFX v18.2. The heat loads adopted for the analyses are based on the most updated data, to return the thermal field for the most recent design.

The study, aimed to optimize the number of channels in the different FW systems, has demonstrated that different FW design can withstand the imposed heat loads and meet the DEMO design requirements.

Both for the equatorial COB and IB, the configuration that features only 4 FW channels is able to keep the structural materials well below their temperature limits and decrease the volume of water in the first centimeters of the cell, a fundamental parameter for a good yield of the TBR. Large and safety margins are present to avoid the arising of thermal crisis, even if subcooled nucleate boiling is expected to happen in limited regions of the cooling system. Furthermore, configuration with 4 channels increases the thermo-hydraulic performance, enhancing the average velocity of the water circuit. Both configurations can be considered as an excellent integration in the current design.

Regarding the IB apical cell, it is not possible to reduce the number of channels due to the highest HF impacting the Tungsten layer, that produces hot spots in the Eurofer structures. As reported, the fixed pitch layout does not satisfy the temperature requirements exceeding the maximum allowable temperature of 550°C by 2.3 degrees and, instead, a variable pitch configuration must be adopted. However, this system is deemed to require further analysis, since the safety margins on the operative temperature limit are remarkably low and are likely to be exceeded even for small fluctuations of the thermal load. Further analyses are required with a non-uniform HF on the Tungsten layer to highlight and delimit the onset of hot-spots. In addition, modeling the eventual phase change, to evaluate the perturbation in the system due to the formation and evolution of steam and the use of different turbulence models, would be a remarkable improvement.

Finally, it has been demonstrated that the COB optimized layout is able to effectively withstand the thermal loads associated with the DEMO ramp-up transient. The FW system promptly reacts to the power variation and rapidly reaches the steady operative conditions (450 s) after the FW water inlet temperature became constant (300 s). This configuration fully withstands the thermal loads during the ramp-up phase. It has been also demonstrated that, even when the reactor reaches full power (100 s) and for off-nominal inlet water temperature, the FW does not present any hot spots.

To provide a more detailed thermal field of the elementary cell, composed by both systems, BZ and FW, further analyses should be performed in the future to evaluate the effects of the mutual interaction between these two systems, and how much this impacts the thermal field. Regarding the transient analysis, further studies will be conducted with both systems, BZ and FW, to consider the real thermal inertia of the system and the large PbLi thermal conductivity. Moreover, analyses should be performed with water inlet mass flow rate variation during the ramp-up to obtain a constant outlet temperature of 328°C, suitable for the PHTS.

Acknowledgments

This work has been carried out within the framework of the EUROfusion Consortium and has received funding from the Euratom research and training programme 2014-2018 and 2019-2020 under grant agreement No 633053. The views and opinions expressed herein do not necessarily reflect those of the European Commission.

References

[1] G. Federici, et al., An overview of the EU breeding blanket design strategy as an integral part of the DEMO design effort, *Fusion Engineering and Des*ign, Vol. 141, 2019, Pages 30-42. DOI: 10.1016/j.fusengdes.2019.01.141

[2] E. Martelli, et al., Advancements in DEMO WCLL breeding blanket design and integration. *Int. J. Energy Res.*, Vol. 42, 2018, Pages 27-52. DOI:10.1002/er.3750

[3] G. Aiello, et al., Assessment of design limits and criteria requirements for Eurofer structures in TBM components, *J. Nucl. Mater.*, 414 (2011), pp. 53-68. DOI: 10.1016/j.jnucmat.2011.05.005

[4] D. Sornin, A. Li Puma, C. Schweier, WPBB-DEL- BB-7.1.1-T003-D001, EFDA D 2NBQ6U, Assessment of Manufacturing Technologies for Blanket Development (WCLL) / 2017 status of WCLL manufacturing activities, Eurofusion, 2018

[5] A. Del Nevo, et al., Recent progress in developing a feasible and integrated conceptual design of the WCLL BB in EUROfusion project, *Fusion Engineering and Design*, Volume 146, Part B, 2019, Pages 1805-1809. DOI:10.1016/j.fusengdes.2019.03.040.

[6] F. Edemetti, et al., On the impact of the heat transfer modelling approach on the prediction of EU-DEMO WCLL breeding blanket thermal performances, *Fusion Engineering and Desing*, paper under review

[7] J. Kecheng, et al., Investigation on cooling performance of WCLL breeding blanket first wall for EU DEMO, *Fusion Engineering and Design*, Volume 146, Pages 2748-2756. DOI: 10.1016/j.fusengdes.2019.05.018.

[8] E. Martelli, et al., Study of EU DEMO WCLL breeding blanket and primary heat transfer system integration, *Fusion Engineering and Design,* Vol. 136, Part B, 2018, Pages 828-833 DOI: 10.1016/j.fusengdes.2018.04.016

[9] S. Noce, et al., Nuclear analysis of the Single Module Segment WCLL DEMO, *Fusion Engineering and Design*, Vol. 147, 2019. DOI:10.1016/j.fusengdes.2019.05.026.

[10] F. Maviglia, et al., Wall protection strategies for DEMO plasma transients, *Fusion Engineering and Design*, Vol. 136, Part A, 2018, Pages 410-414. DOI:10.1016/j.fusengdes.2018.02.064.

[11] F. Maviglia, et al., Overview of DEMO Technology and Scenario Design activities in Europe, *2nd Asia-Pacific Conference on Plasma Physics (AAPPS-DPP 2018)*, Kanazawa, Japan, 12.11.2018 – 17.11.2018.

[12] E. Martelli, et al., Thermo-hydraulic analysis of EU DEMO WCLL breeding blanket. *Fusion Engineering and Design*, 2018 Vol. 130, 48-55. DOI: 10.1016/j.fusengdes.2018.03.030

[13] ISL Inc, RELAP5/MOD3.3 Code Manual Volume I: Code Structure, System Models, and Solution Methods, Nuclear Safety Analysis Division, July 2003

[14] A. Tassone, et al., Recent progress in the WCLL breeding blanket design for the DEMO fusion reactor, *IEEE Transactions on Plasma Science*, Vol. 46, 2018, Pages 1446-1457. DOI:10.1109/TPS.2017.2786046

[15] F. Edemetti, et al., DEMO WCLL breeding zone cooling system design: Analysis and discussion. *Fusion Engineering and Design,* Vol. 146, Part B, 2019, Pages 2632-2638. DOI: 10.1016/j.fusengdes.2019.04.063.

[16] C. Harrington, et al., WCLL BB Extended thermodynamic modelling activities with Apros for simulating DEMO with IHTS & ESS, IDM ref: EFDA_D_2MG38N, Jan 2019

[17] I. Di Piazza, et al., Numerical prediction of turbulent flow and heat transfer in helically coiled pipes, *International Journal of Thermal Sciences*, Volume 49, Issue 4, 2010, Pages 653-663. DOI: 10.1016/j.ijthermalsci.2009.10.001.

[18] E. Martelli, et al., Thermal-hydraulic modeling and analyses of the water-cooled EU DEMO using RELAP5 system code, *Fusion Engineering and Design*, Vol. 146, Part A, 2019, Pages 1121-1125. DOI: 10.1016/j.fusengdes.2019.02.021.

[19] M. Shah, A general correlation for critical heat flux in horizontal channels, *International Journal of Refrigeration*, 2015. DOI:10.1016/j.ijrefrig.2015.06.027.

[20] L.S. Tong, A phenomenological study of critical heat flux, ASME Paper 75-HT-68, 1975